A New Family of Nonstoichiometric Layered Rare-Earth Tin Antimonides, $RESn_xSb_2$ (RE = La, Ce, Pr, Nd, Sm): Crystal Structure of $LaSn_{0.75}Sb_2$

Michael J. Ferguson, Ryan W. Hushagen, and Arthur Mar*

Department of Chemistry, University of Alberta, Edmonton, Alberta, Canada T6G 2G2

Received February 29, 1996[⊗]

A new class of nonstoichiometric layered ternary rare-earth tin antimonides, $RESn_xSb_2$ (RE = La, Ce, Pr, Nd, Sm), has been synthesized through reaction of the elements at 950 °C. In the lanthanum series $LaSn_xSb_2$, tin can be incorporated from a maximum content of $x \approx 0.7$ or 0.8 to as low as $x \approx 0.10$. The structure of lanthanum tin diantimonide with the maximum tin content, $LaSn_{0.75}Sb_2$, has been determined by single-crystal X-ray diffraction methods. It crystallizes in the orthorhombic space group D_{2h}^{17}-*Cmcm* with $a = 4.2425(5)$ Å, $b = 23.121(2)$ Å, $c = 4.5053(6)$ Å, and $Z = 4$. The isostructural rare-earth analogues were characterized by powder X-ray diffraction. The structure of $LaSn_{0.75}Sb_2$ comprises layers of composition "$LaSb_2$" in which La atoms are coordinated by Sb atoms in a square-antiprismatic geometry. Between these layers reside chains of Sn atoms distributed over three crystallographically independent sites, each partially occupied at about 20%. The structure of $LaSn_{0.75}Sb_2$ can be regarded as resulting from the excision of RE−Sb and Sb−Sb bonds in the related structures of binary rare-earth diantimonides, $RESb_2$, and then intercalation of Sn atoms between layers.

Introduction

Low-dimensionality is an important prerequisite for the manifestation of unusual physical properties such as highly anisotropic electrical conductivity (perhaps even superconductivity), charge density waves, or magnetic ordering phenomena and for an extensive intercalation chemistry.[1−3] In two-dimensional structures, for instance, the separation between layers may be characterized by weak van der Waals bonding, as in graphite or layered dichalcogenides, or by an alternation of ionic and covalent bonding, as in the cuprate superconductors. In an effort to steer away from the heavily traversed areas of oxides and chalcogenides, we have directed our search for such low-dimensional compounds among metal antimonides. In particular, we have been investigating ternary rare-earth antimonides *RE*/*M*/Sb in which the second component *M* is a main-group metal, in this case, Sn. Many binary as well as the few known ternary antimonides already adopt low-dimensional structures.[4−7] Moreover, we are propelled by the notion that if even simple binary stannides or antimonides are endowed with such useful physical properties such as superconductivity in $LaSn_3$ or La_4Sb_3[8,9] or have such technologically important applications such as GaSb or InSb in light-emitting diodes or photoconductive IR detectors,[10] then ternary or higher multinary antimonides will provide us with an even greater opportunity for exerting fine steric and electronic control on structures and properties.

We report here our initial results from investigating the La/Sn/Sb system and describe the structure of $LaSn_{0.75}Sb_2$, which forms a member of a new family of nonstoichiometric layered rare-earth tin antimonides. The ternary La/Sn/Sb system appears to have been studied earlier, but not at all comprehensively. Hulliger and Ott reported a ternary La_4SnSb_2 compound in which Sn atoms substitute in a disordered fashion in the parent La_4Sb_3 structure, an antitype of the bcc Th_3P_4 structure.[9] Wang, Steinfink, and Raman studied the "$LaSn_2$"−$LaSb_2$ sections and reported a ternary compound that they tentatively identified as "$LaSnSb_2$".[11] However, they did not pursue the crystal structure determination of this compound and made no further mention of it except to report its X-ray powder pattern and to suggest its probable similarity to the $NdTe_3$ structure.[12] As we will show, the compound identified earlier as "$LaSnSb_2$" is in fact a member of the nonstoichiometric $LaSn_xSb_2$ ($x = \sim 0.1$ to ~ 0.8) series that we fully characterize below. The structure of $LaSn_{0.75}Sb_2$, consisting of one-dimensional Sn chains and two-dimensional Sb sheets, is actually more complicated than being a mere variant of the $NdTe_3$ structure, as was thought. Attempting to describe the nature of the Sn atoms in this structure poses challenging questions as to how bonding of metalloid elements should be viewed and tests the limits on how far the Zintl concept can be applied in systems containing elements of intermediate electronegativity.

Experimental Section

Synthesis. The phase $RESn_xSb_2$ was originally identified in our laboratory as a side product in tin flux reactions intended for the growth of single crystals of RE_3NbSb_5.[5] The persistent presence of this phase in yet other tin flux reactions led us to isolate the single crystals of

[⊗] Abstract published in *Advance ACS Abstracts,* July 1, 1996.

(1) *Electronic Structure and Electronic Transitions in Layered Materials*; Grasso, V., Ed.; Physics and Chemistry of Materials with Low-Dimensional Structures, Series A; D. Reidel: Dordrecht, The Netherlands, 1986.
(2) *Crystal Chemistry and Properties of Materials with Quasi-One-Dimensional Structures*; Rouxel, J., Ed.; Physics and Chemistry of Materials with Low-Dimensional Structures, Series B; D. Reidel: Dordrecht, The Netherlands, 1986.
(3) *Intercalation Chemistry*; Whittingham, M. S., Jacobson, A. J., Eds.; Academic Press: New York, 1982.
(4) Brylak, M.; Jeitschko, W. *Z. Naturforsch., B* **1995**, *50*, 899.
(5) Bolloré, G.; Ferguson, M. J.; Hushagen, R. W.; Mar, A. *Chem. Mater.* **1995**, *7*, 2229.
(6) Sologub, O.; Noël, H.; Leithe-Jasper, A.; Rogl, P.; Bodak, O. I. *J. Solid State Chem.* **1995**, *115*, 441.
(7) Brylak, M.; Möller, M. H.; Jeitschko, W. *J. Solid State Chem.* **1995**, *115*, 305.
(8) Havinga, E. E.; Damsma, H.; van Maaren, M. H. *J. Phys. Chem. Solids* **1970**, *31*, 2653.
(9) Hulliger, F.; Ott, H. R. *J. Less-Common Met.* **1977**, *55*, 103.
(10) *Concise Encyclopedia of Semiconducting Materials and Related Technologies*; Mahajan, S., Kimerling, L. C., Eds.; Pergamon Press: Oxford, U.K., 1992.
(11) Wang, R.; Steinfink, H.; Raman, A. *Inorg. Chem.* **1967**, *6*, 1298.
(12) Norling, B. K.; Steinfink, H. *Inorg. Chem.* **1966**, *5*, 1488.

S0020-1669(96)00225-X CCC: $12.00

$LaSn_{0.75}Sb_2$ ultimately used in the structure determination. These crystals were obtained from a reaction of a 0.5-g mixture of the elements La, Si, and Sb in a 2:2:5 ratio to which a large excess of Sn was added (La, 74 mg, 0.53 mmol, 99.9%, Aesar; Si, 15 mg, 0.53 mmol, 99.96%, Cerac; Sb, 161 mg, 1.33 mmol, 99.999%, Cerac; Sn, 321 mg, 2.70 mmol, 99.8%, Cerac). The reactants were ground together and loaded into a quartz tube (8-cm length; 10-mm i.d.) that was then evacuated and sealed. The sample was heated at 570 °C for 1 day and at 950 °C for 2 days and was then cooled to room temperature over 1 day. The excess Sn was dissolved with concentrated HCl, and the product was found to contain silvery flat needle-shaped crystals. EDX analysis (energy-dispersive X-ray analysis) on these crystals with a JEOL JSM-6301FXV field-emission scanning electron microscope revealed the presence of the elements La, Sn, and Sb (but *no* Si) in the approximate ratio 1:<1:2, with a deficiency of Sn consistently observed. The Si apparently remained unreacted, as revealed from powder X-ray analysis of the product. The crystal structure determination (*vide infra*) ultimately established the stoichiometry, which was confirmed by quantitative EDX analyses with a JEOL 8900 microprobe. Anal. Calcd for $LaSn_{0.75}Sb_2$: La, 29.5; Sn, 18.9; Sb, 51.6. Found (average of 10 analyses): La, 30.8(3); Sn, 17.3(5); Sb, 49.1(4).

Since the crystal structure suggested variable Sn occupancy, investigations were carried out to determine the extent to which Sn can be incorporated into the structure, as well as to confirm if rational syntheses of these compounds are possible. A series of 0.5-g samples were prepared from mixtures of the elements according to La + xSn + 2Sb (where x = 0, 0.10, 0.20, ..., 1.00, 2.00). Here, Sn is now considered to serve as an actual reactant rather than merely as a nonreactive flux. The samples were loaded into quartz tubes as before and heated using the same temperature profile as indicated above. These reactions resulted in the formation of the desired ternary phase (with the exception, of course, of the control sample with x = 0, which gave the expected $LaSb_2$), as detected by X-ray powder patterns obtained on an Enraf-Nonius FR552 Guinier camera (Cu Kα_1 radiation; Si standard). The cell parameters were refined by least-squares fits of typically 20−35 reflections in the powder patterns with the use of the program POLSQ.[13]

In a similar fashion, rare-earth substitutions were carried out by preparing 0.5-g samples containing mixtures of the elements *RE*, Sn, and Sb in the ratio 1:0.5:3 (where *RE* = La, Ce, Pr, Nd, Sm, and Gd), which were then heated as before. In all cases except for *RE* = Gd (which gave only known binary phases), needle-shaped crystals with metallic luster were obtained, which were verified by EDX analyses to be the desired ternary compounds. These compounds are stable indefinitely in air. Subsequently, reactions with starting composition *RE*$SnSb_2$ (*RE* = La, Ce, Pr, Nd, Sm) were carried out, which we assume yield the ternary phase with the maximum Sn content; these products were characterized by powder X-ray diffraction as well.

Structure Determination of $LaSn_{0.75}Sb_2$. Preliminary cell parameters were determined from Weissenberg photographs, which revealed Laue symmetry *mmm* and systematic extinctions (*hkl*, $h + k = 2n + 1$; *h*0*l*, $l = 2n + 1$) consistent with the orthorhombic space groups D_{2h}^{17}-*Cmcm*, C_{2v}^{12}-*Cmc*2_1, and C_{2v}^{16}-*C*2*cm*. Final cell parameters were determined from a least-squares analysis of the setting angles of 34 reflections in the range 22° ≤ 2θ(Mo Kα) ≤ 28° centered on a Siemens P4RA diffractometer. Intensity data were collected at −60 °C with the $\theta-2\theta$ scan technique in the range 2° ≤ 2θ(Mo Kα) ≤ 70°. Three standard reflections monitored at intervals of every 100 reflections showed no significant change during the data collection. Crystal data are given in Table 1, and further details are given in Table S1 of the Supporting Information.

Calculations were carried out with the use of programs in the SHELXTL (Version 5.0) package.[14,15] Conventional atomic scattering factors and anomalous dispersion corrections were used.[16] Intensity data were reduced and averaged, and face-indexed Gaussian-type absorption corrections were applied with the use of the program XPREP. Intensity statistics and satisfactory averaging (R_{int} = 0.034) favored the centrosymmetric space group *Cmcm*. Initial positions of the La and Sb atoms were found by direct methods with the program XS. The ensuing difference Fourier syntheses persistently revealed additional electron density located between the layers of composition "$LaSb_2$". Introduction of a site at 0, 0, 0 that was permitted to be partially occupied by Sn atoms could account for this electron density, but this model was deemed unsatisfactory because it resulted in a highly elongated thermal ellipsoid for this site that stretches along the *c* direction. Restriction of the displacement parameter of this site to a more reasonable, isotropic value allowed two additional sites, at 0, *y*, $^1/_4$ and 0, *y*, *z*, to be resolved in the difference Fourier map. Together, these three closely-split sites were allowed to be partially occupied by Sn atoms, but their thermal motion was constrained to be isotropic. There is no justification for introducing anisotropy for the Sn atoms given that values of the site occupation factors and displacement parameters are expected to be highly correlated in the least-squares refinements.

Table 1. Crystallographic Data for $LaSn_{0.75}Sb_2$

formula $LaSn_{0.75}Sb_2$	D_{2h}^{17}-*Cmcm* (No. 63)
fw 471.43	T = −60 °C
a = 4.2435(5) Å[a]	λ = 0.710 73 Å
b = 23.121(2) Å[a]	ρ_{calc} = 7.084 g cm^{-3}
c = 4.5053(6) Å[a]	μ = 255.4 cm^{-1}
V = 442.03(5) Å^3	$R(F)$ for $F_o^2 > 2\sigma(F_o^2)$[b] = 0.028
Z = 4	$R_w(F_o^2)$[c] = 0.067

[a] Obtained from a refinement constrained so that $\alpha = \beta = \gamma = 90°$. [b] $R(F) = \sum||F_o| - |F_c||/\sum|F_o|$. [c] $R_w(F_o^2) = [\sum(w(F_o^2 - F_c^2)^2]/\sum wF_o^4]^{1/2}$; $w^{-1} = [\sigma^2(F_o^2) + (0.026p)^2 + 8.62p]$ where $p = [\max(F_o^2,0) + 2F_c^2]/3$.

To minimize artifacts that may be associated with such correlations, refinements at this stage were performed very gradually and not indiscriminately. The displacement and then the site occupation factor of one Sn site were allowed to refine while all parameters associated with the other two Sn sites were fixed. This procedure was repeated in turn for all the Sn sites. In the final stage, the site occupation and displacement parameters of *all* three Sn sites were left unconstrained and allowed to refine freely. These converged in a well-behaved manner to reasonable values notwithstanding the relatively unencumbered stage of this refinement. We interpret this result as strong evidence for the existence of three distinct, partially occupied interlayer sites, as opposed to an ill-defined smearing of electron density. We attempted to formulate models in which these Sn atoms fully occupied sites in an ordered fashion in the lower symmetry space group *Cmc*2_1 but found no evidence to support these.

The possibility of disorder between Sn and Sb atoms was considered. Given the similar scattering powers of Sn and Sb, however, it is not surprising that they cannot be distinguished with the available X-ray data. Later, we will present chemical arguments *against* a disordered Sn/Sb model. A refinement in which the occupancies of *all* atoms were unconstrained resulted in values of 100(3)% for La, 100(3)% for Sb(1), 99(3)% for Sb(2), 18.6(7)% for Sn(1), 18.1(8)% for Sn(2), and 19.7(9)% for Sn(3). This results in the formula $La_{1.00(3)}Sn_{0.75(3)}Sb_{1.99(3)}$ (the multiplicity of the Sn(1) site is twice that of the Sn(2) or Sn(3) sites). We thus accept the formulation $LaSn_{0.75}Sb_2$, which agrees well with the chemical analysis obtained independently (*vide supra*).

The final cycle of least-squares refinement on F_o^2 of 23 variables (including anisotropic displacement parameters for the La and Sb atoms, site occupation factors for the Sn atoms, and an isotropic extinction parameter) and 592 averaged reflections (including those having F_o^2 < 0) converged to residuals of $R_w(F_o^2)$ of 0.067 and $R(F)$ (for $F_o^2 > 2\sigma(F_o^2)$) of 0.028. The final difference electron density map is featureless ($\Delta\rho_{max}$ = 1.8, $\Delta\rho_{min}$ = −3.6 e Å^{-3}). The atomic positions were standardized with the program STRUCTURE TIDY.[17] Final values of the positional and displacement parameters are given in Table 2. Anisotropic displacement parameters are given in Table S2 (Supporting Information), and final structure amplitudes are available from A.M.

(13) POLSQ: Program for least-squares unit cell refinement. Modified by D. Cahen and D. Keszler, Northwestern University, 1983.
(14) Sheldrick, G. M. *SHELXTL*, Version 5.0; Siemens Analytical X-ray Instruments, Inc.: Madison, WI, 1994.
(15) Sheldrick, G. M. *J. Appl. Crystallogr.*, in press.
(16) *International Tables for X-ray Crystallography*; Wilson, A. J. C., Ed.; Kluwer: Dordrecht, The Netherlands 1992; Vol. C.
(17) Gelato, L. M.; Parthé, E. *J. Appl. Crystallogr.* **1987**, *20*, 139.

Table 2. Atomic Coordinates, Occupancies, and Equivalent Isotropic Displacement Parameters (Å^2) for $LaSn_{0.75}Sb_2$

atom	Wyckoff position	x	y	z	occ	U_{eq}[a]
La	4c	0	0.86085(2)	1/4	1	0.0062(1)
Sb(1)	4c	0	0.24860(2)	1/4	1	0.0071(2)
Sb(2)	4c	0	0.59076(2)	1/4	1	0.0081(2)
Sn(1)	8f	0	0.0065(1)	0.1238(6)	0.186(4)	0.0114(8)[b]
Sn(2)	4c	0	0.0089(1)	1/4	0.181(6)	0.010(1)[b]
Sn(3)	4a	0	0	0	0.197(6)	0.013(1)[b]

[a] U_{eq} is defined as one-third of the trace of the orthogonalized $\boldsymbol{U}_{ij}$ tensor. [b] The Sn atoms were refined isotropically.

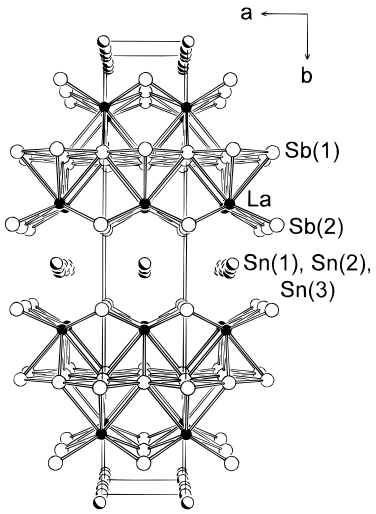

Figure 1. View down the *c* axis of $LaSn_{0.75}Sb_2$ with the unit cell outlined. The solid circles are La atoms, and the open circles are Sb atoms. The partly shaded circles, however, merely represent *sites* for the Sn atoms and do not imply the actual presence of the atoms themselves. The Sn sites are better seen in Figures 2 and 3.

Electrical Resistivity. Single crystals of $LaSn_{0.75}Sb_2$ (from the same batch used in the structure determination) ranging in length from 0.8 to 1.4 mm were mounted with Ag paint on Au wires with graphite extensions. Four-probe ac electrical resistivity measurements were made down to 20 K, along the needle axis *a* of these crystals. The small cross-sectional dimensions of these crystals preclude measurements along the other directions.

Results and Discussion

Description of the Structure. A view of the structure of $LaSn_{0.75}Sb_2$ down the *c* axis is given in Figure 1, which also shows the labeling scheme. Selected interatomic distances and angles are given in Table 3. The compound $LaSn_{0.75}Sb_2$ adopts a novel layered structure type that comprises layers of composition $^2_\infty[LaSb_2]$ lying parallel to the (010) plane. These layers are separated by an unusual arrangement of Sn atoms partially occupying sites aligned along the *c* axis (Figure 2). The La atoms are coordinated by eight Sb atoms in a square-antiprismatic fashion, as shown in Figure 3. Four Sb(1) atoms at distances of 3.3523(6) (2×) and 3.3879(5) Å (2×) define one square of Sb atoms. Four Sb(2) atoms at distances of 3.2905(4) Å (4×) define a larger square twisted 45° relative to the first square. The Sb(1) atoms are surrounded by four other symmetry-equivalent Sb(1) atoms forming a nearly flat square sheet $^2_\infty[Sb]$, with Sb(1)−Sb(1)−Sb(1) angles of 177.60(4), 86.55(1), and 93.40(1)° and Sb(1)−Sb(1) distances of 3.0952(3) Å (4×). The La square antiprisms are then positioned above and below this infinite Sb(1) square sheet in a checkerboard pattern to form the $^2_\infty[LaSb_2]$ layers.

A view of the structure down the *a* axis, perpendicular to the previous view, shows the wavelike pattern of the Sn sites

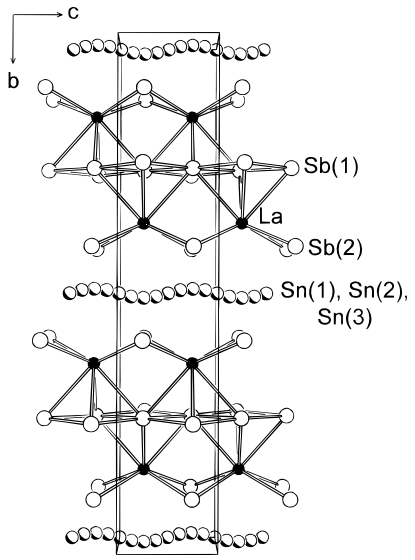

Figure 2. View down the *a* axis of $LaSn_{0.75}Sb_2$ showing the wavelike arrangement parallel to the *c* direction of the three Sn sites positioned between the layers of composition $LaSb_2$. It must be stressed that these sites are only *partially* occupied, each at about 20%. (See text for fuller discussion.)

Table 3. Selected Interatomic Distances (Å) and Angles (deg) for $LaSn_{0.75}Sb_2$

La−Sb(2)	3.2905(4) (4×)	Sb(1)−Sb(1)	3.0952(3) (4×)
La−Sb(1)	3.3523(6) (2×)	Sn(1)−Sb(2)	2.936(2) (2×)
La−Sb(1)	3.3879(5) (2×)	Sn(1)−Sb(2)	3.521(2) (2×)
La−Sn(3)	3.4087(5) (2×)	Sn(1)−Sn(3)	2.814(3)
La−Sn(1)	3.415(2) (2×)	Sn(1)−Sn(2)	2.844(3)
La−Sn(2)	3.423(3)	Sn(2)−Sb(2)	2.843(2) (2×)
La−Sn(1)	3.499(2) (2×)	Sn(2)−Sb(2)	3.858(2) (4×)
La−Sn(2)	3.761(3) (3×)	Sn(3)−Sb(2)	3.1897(4) (4×)

Sb(2)−La−Sb(2)	140.25(2)	La−Sb(2)−La	80.3(1)
Sb(2)−La−Sb(2)	80.30(1)	La−Sb(2)−La	140.2(2)
Sb(2)−La−Sb(2)	86.41(1)	La−Sb(2)−La	86.4(1)
Sb(2)−La−Sb(1)	132.17(1)	Sb(2)−Sn(1)−Sb(2)	92.54(7)
Sb(2)−La−Sb(1)	81.67(1)	Sb(2)−Sn(1)−Sn(2)	83.74(8)
Sb(2)−La−Sb(1)	135.16(1)	Sb(2)−Sn(1)−Sn(3)	103.22(7)
Sb(2)−La−Sb(1)	78.39(1)	Sn(2)−Sn(1)−Sn(3)	169.8(1)
Sb(1)−La−Sb(1)	78.53(2)	Sb(2)−Sn(2)−Sb(2)	96.5(1)
Sb(1)−La−Sb(1)	54.67(1)	Sb(2)−Sn(2)−Sn(1)	94.78(5)
Sb(1)−La−Sb(1)	83.35(2)	Sn(1)−Sn(2)−Sn(1)	165.6(1)
Sb(1)−Sb(1)−Sb(1)	177.60(4)	Sb(2)−Sn(3)−Sb(2)	83.4(1)
Sb(1)−Sb(1)−Sb(1)	86.55(1)	Sb(2)−Sn(3)−Sb(2)	96.6(1)
Sb(1)−Sb(1)−Sb(1)	93.40(1)	Sb(2)−Sn(3)−Sb(2)	180
La−Sb(1)−La	78.53(2)	Sn(1)−Sn(3)−Sn(1)	180
La−Sb(1)−La	125.33(1)		
La−Sb(1)−La	83.35(2)		

(Figure 2). It must be strongly emphasized that these sites are only *partially* occupied (each at ∼20%), as adjacent sites are obviously too close (<0.6 Å) for them to be fully occupied simultaneously. As shown in Figure 3, there are three distinct sites with Sn(1) in a position of twice the multiplicity as that of Sn(2) or Sn(3), giving rise to an ordering of ...Sn(2)−Sn(1)−Sn(3)−Sn(1)... for the arrangement of these sites. The distances from these Sn sites to the La atom range from 3.4087(5) to 3.761(3) Å.

Located in the interlayer regions, the Sn atoms must be coordinated by the surrounding Sb(2) atoms. The Sn(1) site has two Sb(2) atoms at 2.936(2) Å on one side of it, subtending an angle of 92.54(7)° (Figure 4a). On the other side are two more Sb(2) atoms considerably further away, at 3.521(2) Å. Similarly, the Sn(2) site has two Sb(2) atoms at a short distance, 2.843(2) Å, subtending an angle of 96.5(1)° (Figure 4b). The four next nearest Sb(2) atoms are far away at 3.858(2) Å. Finally, the Sn(3) site is surrounded by four Sb(2) atoms at

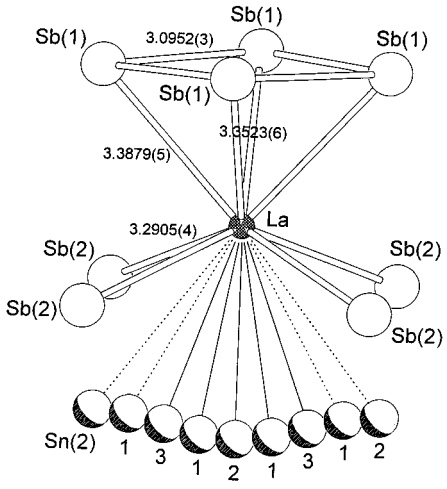

Figure 3. Coordination of the La atom in $LaSn_{0.75}Sb_2$, with the square-antiprismatic geometry of the Sb atoms shown and the La−Sb and Sb−Sb bond lengths indicated. The capping Sn sites beneath the La atom are labeled. In order from left to center, the La−Sn distances are 3.761(3) Å to Sn(2), 3.499(2) Å to Sn(1), 3.4087(5) Å to Sn(3), 3.415(2) Å to Sn(1), and 3.423(3) Å to Sn(2).

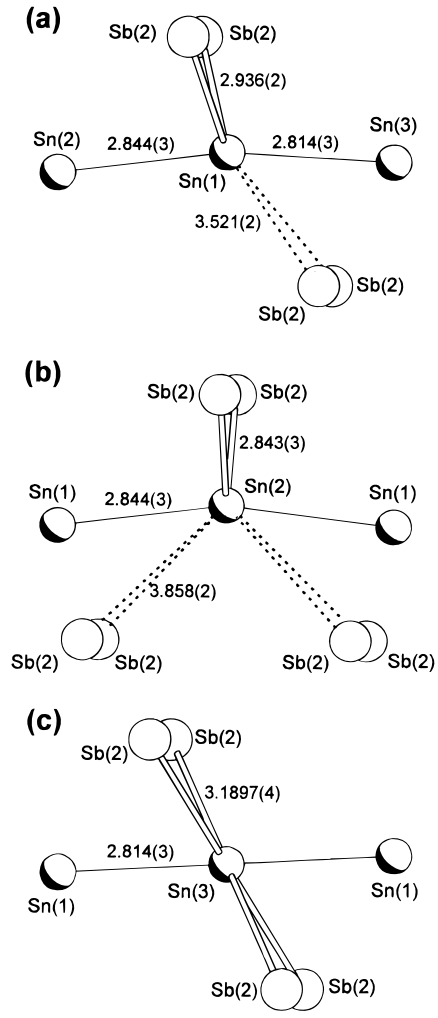

Figure 4. Coordination of the Sn atoms in $LaSn_{0.75}Sb_2$: (a) Sn(1) site; (b) Sn(2) site; (c) Sn(3) site. The Sn atoms at appropriate distances for possible bonding interactions (∼2.8 Å) are also shown. See text for interpretation.

3.1897(4) Å in a nearly square-planar fashion (Figure 4c). With the Sn sites spaced at increments of ∼0.5−0.6 Å from each other, all the generated Sn−Sn distances are unreasonable for bonding except for those in the vicinity of ∼2.8 Å. In other words, one possible model that can be invoked to interpret the ∼20% occupancy of *each* site is to suggest that every *fifth* site (or further) is fully occupied on a local level. Figure 4 shows the nearly linear coordination of the Sn atoms by other Sn atoms within this reasonable bonding range (2.814(3)−2.844(3) Å); the subtended angles range from 165.6(1) to 180°.

Table 4. Cell Parameters for Ternary $LaSn_{0.75}Sb_2$-Type Compounds Obtained from the Reactions La + *x*Sn + 2Sb

loading compn	*a* (Å)	*b* (Å)	*c* (Å)	*V* (Å^3)
$LaSn_{0.10}Sb_2$	4.276(1)	23.090(4)	4.459(1)	440.2(1)
$LaSn_{0.20}Sb_2$	4.271(2)	23.100(9)	4.460(2)	440.1(2)
$LaSn_{0.30}Sb_2$	4.265(1)	23.128(5)	4.474(1)	441.4(1)
$LaSn_{0.40}Sb_2$	4.260(1)	23.119(6)	4.477(1)	440.9(1)
$LaSn_{0.50}Sb_2$	4.259(1)	23.139(5)	4.485(1)	442.0(1)
$LaSn_{0.60}Sb_2$	4.256(1)	23.120(5)	4.492(1)	442.0(1)
$LaSn_{0.70}Sb_2$	4.253(1)	23.140(3)	4.498(1)	442.7(1)
$LaSn_{0.80}Sb_2$	4.248(1)	23.128(6)	4.499(1)	442.1(1)
$LaSn_{0.90}Sb_2$	4.249(1)	23.130(4)	4.505(1)	442.7(1)
$LaSn_{1.00}Sb_2$	4.247(1)	23.139(6)	4.504(1)	442.6(1)
$LaSn_{2.00}Sb_2$	4.248(1)	23.135(5)	4.505(1)	442.7(1)

Nonstoichiometry of Sn. Since the original synthesis producing the crystals for the structure determination involved a large excess of Sn, the amount of Sn actually incorporated into the compound $LaSn_{0.75}Sb_2$ must represent a maximum limiting value. Is the Sn content variable? To determine the degree of nonstoichiometry in this phase, a series of reactions, La + *x*Sn + 2Sb ($x = 0-2.0$), were performed. Not surprisingly, the control experiment, La + 0Sn + 2Sb, resulted in phase-pure $LaSb_2$.[18] More remarkably, however, the ternary phase could be formed as essentially the pure product (>95%) in all the other preparations, as observed in the X-ray powder patterns, even down to as low as $x = 0.1$. With $x \geq 0.8$, excess Sn and other unidentified phases can begin to be detected as minor impurities. The cell parameters refined from the powder data are listed in Table 4.

The variation in the cell parameters as a function of *x* is small but is readily discernible in the case of the *a* and *c* parameters, as shown in Figure 5. The *b* parameter and the unit cell volume, however, do not exhibit as much variation. A number of important conclusions can be drawn from these data. Most significantly, the *a* parameter decreases while the *c* parameter increases steadily with increasing *x*, eventually reaching a plateau at approximately $x = 0.7$ or 0.8. With greater quantities of Sn loaded in the preparation, the cell parameters no longer change. This implies that $x = 0.7$ or 0.8 also corresponds to the maximum Sn content. Note that this value agrees precisely with the formula obtained independently from the crystal structure, $LaSn_{0.75(3)}Sb_2$. The cell parameters refined from the single-crystal data (Table 1) also agree reasonably well with those from the powder data for $LaSn_{0.7}Sb_2$ or $LaSn_{0.8}Sb_2$ (Table 4). During the structure refinement, we pointed out the difficulty in distinguishing between the Sn and Sb atoms. The observation of limiting values for the cell parameters at a stoichiometry consistent with the single-crystal formula argues strongly for an ordered model. The X-ray powder pattern for the preparation $LaSn_{0.7}Sb_2$ matches well with the predicted pattern calculated from the structure determined from the single-crystal data (Table 5). Other related reactions that we have carried out in this laboratory support this model. For instance, using now an excess of *antimony* instead of tin, the reaction La + 0.5Sn + 3Sb led to the formation of crystals that were shown by quantitative microprobe analysis to contain the correct proportion of Sn. Anal. Calcd for $LaSn_{0.5}Sb_2$: La, 31.4; Sn, 13.4; Sb, 55.1. Found (average of 10 analyses): La, 29.8(5); Sn, 12.6(1); Sb, 57.9(5).

(18) Wang, R.; Steinfink, H. *Inorg. Chem.* **1967**, *6*, 1685.

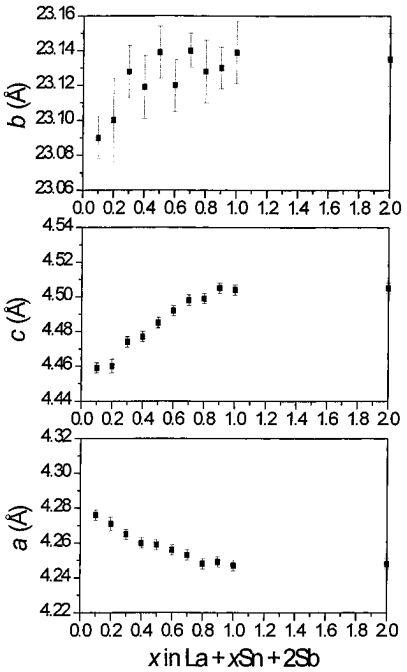

Figure 5. Plots of the cell parameters of the ternary $LaSn_{0.75}Sb_2$-type compounds obtained as a function of amount of Sn used, *x*, in the reaction La + *x*Sn + 2Sb. Note the attainment of a plateau at $x = 0.7$ or 0.8, most readily seen for the *c* or *a* parameter, corresponding to the maximum Sn content.

Table 5. X-ray Powder Diffraction Data for Starting Composition $LaSn_{0.7}Sb_2$

hkl	d_{obs} (Å)	d_{calc} (Å)	I/I_0[a]	*hkl*	d_{obs} (Å)	d_{calc} (Å)	I/I_0[a]
110	4.180	4.183	8	152	1.825	1.827	2
060	3.856	3.857	4	241		1.824	7
041	3.549	3.551	20	082	1.774	1.775	6
150	3.130	3.132	19	0,12,1		1.772	6
111	3.064	3.063	2	261	1.720	1.721	3
061	2.927	2.928	6	280	1.714	1.713	11
080	2.892	2.893	24	172	1.704	1.704	10
131	2.868	2.869	100	281	1.602	1.601	9
170	2.609	2.610	36	0,14,1	1.552	1.551	5
151	2.569	2.570	41	202	1.545	1.545	14
081	2.433	2.433	14	1,13,1		1.542	5
002	2.250	2.249	20	1,11,2	1.445	1.445	13
022	2.208	2.208	3	262	1.435	1.434	5
200	2.126	2.127	27	2,12,0	1.428	1.429	5
042	2.095	2.096	2	133	1.391	1.391	15
0,10,1	2.058	2.058	3	1,15,1	1.380	1.380	10
191	1.977	1.977	6	282	1.363	1.363	6
062	1.943	1.943	6	2,12,1		1.362	6
0,12,0	1.927	1.928	5	153		1.352	7
1,11,0	1.886	1.886	6	331	1.332	1.332	13

[a] The intensities were calculated from the crystal structure of $LaSn_{0.75}Sb_2$ with the use of the program LAZY-PULVERIX (Yvon, K.; Jeitschko, W.; Parthé, E. *J. Appl. Crystallogr.* **1977**, *10*, 73−74.)

Steric considerations would generally lead to the assumption that an increase in the Sn content should be accompanied by an increase in unit cell volume, but this is not the case here. The *b* parameter exhibits little variation, and this may be rationalized by inspecting Figure 1. When even a small amount of Sn is placed between the layers, it already fixes the interlayer spacing by virtue of a "pillaring" action. Apparently it is sufficient for a few initially placed Sn atoms to be located strategically in such a way as to buttress the layers apart at a fixed spacing; further addition of Sn atoms then has little effect on the *b* parameter. The increase of the *c* parameter with increasing Sn content can be explained by arguing that electrostatic repulsions are enhanced within the chains aligned along the *c* direction (Figure 2). In contrast, the *a* parameter *decreases* with increasing Sn content, a rather surprising result. This can be explained on steric grounds if we postulate that the Sn atoms enter the structure with an initial preference for specific sites that bind the surrounding Sb(2) atoms at a further distance than in the final arrangement of $LaSn_{0.75}Sb_2$. Alternatively, there are likely to be more subtle electronic reasons that are not obvious from a simple analysis. In any case, given that both the contraction in *a* (−0.7%) and the expansion in *c* (+0.9%) are small on going from $LaSn_{0.1}Sb_2$ to $LaSn_{0.8}Sb_2$, these explanations should be accepted guardedly pending further experiments.

Structural Relationships and Bonding. The compound $LaSn_{0.75}Sb_2$ bears important structural relationships with the family of known rare-earth diantimonides, $RESb_2$ (Figure 6). All of these structures contain rare-earth atoms in square-antiprismatic coordination. These square antiprisms are condensed to form infinite layers consisting of rare-earth atoms above and below a nearly square net of Sb atoms. These layers are then stitched together through the formation of interlayer Sb−Sb bonds to form the three-dimensional frameworks of $RESb_2$. Formally, the structure of $LaSn_{0.75}Sb_2$ is derived from those of the binary $RESb_2$ compounds by (1) excision of these interlayer Sb−Sb bonds and (2) intercalation of Sn atoms between the separated layers.

It is instructive to review some of these structural features in more detail, as they will help provide useful starting notions of the bonding picture in $LaSn_{0.75}Sb_2$. The $LaSb_2$-type structure is adopted by the early rare-earth diantimonides $RESb_2$ (*RE* = La, Ce, Pr, Nd, Sm) (Figure 6a).[18,19] Even though the actual structure was determined for $SmSb_2$,[18] we shall accept the designation "$LaSb_2$-type" because it is now firmly entrenched in the literature. The layers in $SmSb_2$ are joined by short Sb−Sb *pairs* (2.79(2) Å), corresponding to strong two-electron single bonds in which an oxidation state of Sb^{2-} is attained. The Sb−Sb distances in the nearly square net range from 3.03(2) to 3.09(2) Å.[20] Such distances have been postulated to correspond to one-electron bonds, of 0.5 bond order, leading to an assignment of Sb^- for these atoms.[21,22] The formulation $RE^{3+}Sb^-Sb^{2-}$ for the $LaSb_2$-type structure is thus consistent with the usual Zintl concepts. A capping Sb atom 3.48(2) Å away in the adjacent layer completes the 9-fold monocapped square antiprismatic coordination of the Sm atoms, which are condensed together between layers. The structures of $EuSb_2$ and $YbSb_2$ represent alternative ways of bond formation in response to the replacement of the trivalent rare-earth atom in the $LaSb_2$-type structure by a divalent one. In $EuSb_2$, the rare-earth layers slide relative to each other so as to form infinite zigzag Sb−Sb chains instead of pairs to hold the layers together; the Sb−Sb distance increases to 2.931(3) Å (Figure 6b).[23] Moreover, the square Sb net now becomes puckered and skewed so as to form parallel zigzag Sb−Sb chains: each two-connected Sb atom forms Sb−Sb bonds of 2.924(3) Å. If all the Sb−Sb bonds in $EuSb_2$ are considered to be full two-electron single bonds, the resulting assignment is $Eu^{2+}Sb^-Sb^-$. In $YbSb_2$, which adopts the $ZrSi_2$-type structure, the same type of zigzag Sb−Sb chains holds the rare-earth layers together, with Sb−Sb distances of 2.97(1) Å (Figure 6c).[24] But the square Sb net contains four equally weak one-electron Sb−Sb half-bonds, each of a distance

(19) Eatough, N. L.; Hall, H. T. *Inorg. Chem.* **1969**, *8*, 1439.
(20) Some of the bond lengths reported by Wang and Steinfink are incorrect.[18] The atomic positions, however, are correct.[19]
(21) Brylak, M.; Jeitschko, W. *Z. Naturforsch., B* **1994**, *49*, 747.
(22) Garcia, E.; Corbett, J. D. *J. Solid State Chem.* **1988**, *73*, 452.
(23) Hulliger, F.; Schmelczer, R. *J. Solid State Chem.* **1978**, *26*, 389.
(24) Wang, R.; Bodnar, R.; Steinfink, H. *Inorg. Chem.* **1966**, *5*, 1468.

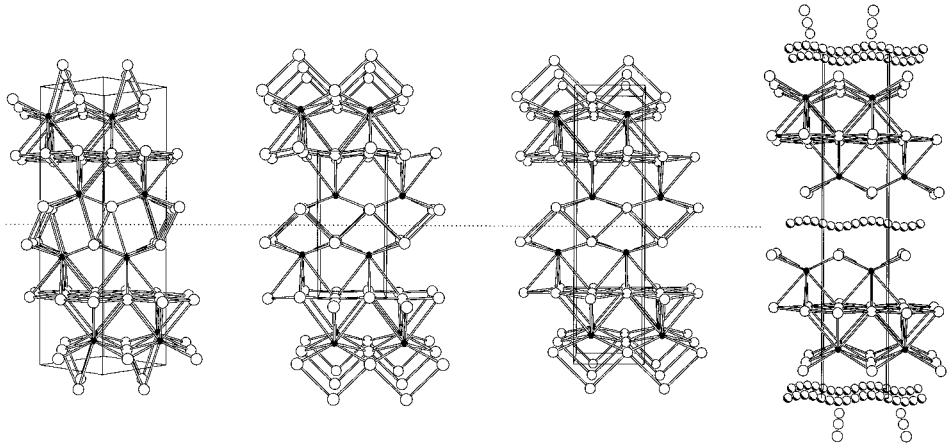

Figure 6. Comparison of various rare-earth diantimonide $RESb_2$ structures and the $LaSn_{0.75}Sb_2$ structure. The solid circles are *RE* atoms, the open circles are Sb atoms, and, in the case of $LaSn_{0.75}Sb_2$, the partly shaded circles are Sn atoms. Note the progressive breaking of interlayer bonds (horizontal dotted line) in the $RESb_2$ structures followed by the insertion of Sn atoms to form the $LaSn_{0.75}Sb_2$ structure.

of 3.12(1) Å. Here, too, the assignment is $Yb^{2+}Sb^{-}Sb^{-}$. At the extreme of this progression, $LaSn_{0.75}Sb_2$ adopts a structure that is most directly related to that of $YbSb_2$: the bonds in the Sb−Sb zigzag chains are broken and the Sn atoms are put in their place (Figure 6d). The stacking axis *b* has been considerably expanded, from 16.63(1) Å in $YbSb_2$ to 23.121(2) Å in $LaSn_{0.75}Sb_2$. The Sb−Sb distances in the square net, 3.095(1) Å, in $LaSn_{0.75}Sb_2$ are close to those in $YbSb_2$, 3.12(1) Å. Accepting the validity of a half-bond approximation, we assign the Sb(1) atoms in the square net to be Sb^{-}. Breaking the bonds in the Sb−Sb zigzag chain holding the layers together in $YbSb_2$ causes the Sb(2) atoms to revert back to Sb^{3-} in $LaSn_{0.75}Sb_2$. We are then left with a puzzling predicament: What is the oxidation state of Sn if we accept, so far, the formulation $(La^{3+})(Sn^{?})_{0.75}(Sb(1)^{-})(Sb(2)^{3-})$? Is $Sn^{1.5+}$ plausible? The apparent breakdown of the Zintl concept here arises from our insistence on assigning only integral oxidation states to the Sb atoms,[25] which we believe are prone to participate in intermediate Sb−Sb interactions. Moreover, the nature of the Sn atoms in $LaSn_{0.75}Sb_2$ is not well-understood at this time. The distances from the Sn atoms to the Sb atoms that sandwich them above and below (2.936(2)−3.190(1) Å) (Figure 4) are similar to, if somewhat longer than, the Sn−Sb distances found in Na_8SnSb_4 (2.843(1) Å),[26] Na_5SnSb_3 (2.805(1)−2.945(1) Å),[27] K_8SnSb_4 (2.898(1) Å),[27] and KSnSb (2.883(2) Å)[28] (*Cf.* ∼2.8 Å for the sum of the covalent radii of Sn and Sb atoms[29]). Although we describe the Sn atoms as occupying, on average, about 20% of all the available sites, we noted earlier that a local interpretation is possible in which Sn atoms occupying every fifth site are at a reasonable distance to participate in Sn−Sn bonding (2.814(3)−2.844(3) Å); these distances are intermediate between those found in gray tin (2.80 Å) and white tin (3.02−3.18 Å).[30] An alternative explanation is to accept Sn^{2+} as the most reasonable oxidation state for tin and postulate that the oxidation states of the Sb atoms are adjusted accordingly in response. This model would then predict that the Sb−Sb bond lengths are sensitive to the Sn content in $LaSn_xSb_2$. This is reflected in the variation of the cell parameters (Table 4), but steric considerations are of course intimately involved as well. Mössbauer or EXAFS data would greatly aid in unraveling the nature of the Sn and Sb atoms.

Table 6. Cell Parameters for Ternary $LaSn_{0.75}Sb_2$-Type Compounds Obtained from the Reactions *RE* + Sn + 2Sb

loading compn	*a* (Å)	*b* (Å)	*c* (Å)	*V* (Å^3)
$LaSnSb_2$	4.246(1)	23.132(6)	4.507(1)	442.6(1)
$CeSnSb_2$	4.228(1)	22.868(4)	4.478(1)	433.0(1)
$PrSnSb_2$	4.204(1)	22.700(7)	4.469(2)	426.5(2)
$NdSnSb_2$	4.195(1)	22.606(5)	4.449(1)	422.0(1)
$SmSnSb_2$	4.174(1)	22.384(5)	4.416(1)	412.6(1)

Another structural consequence induced by the presence of the Sn atoms is that the La atoms are now coordinated by a ninth atom, forming a monocapped square-antiprismatic geometry. Depending on the occupation of the Sn sites, the capping Sn atom may be directly beneath the La atom, at 3.423(3) Å, or it may be tilted progressively to one side, at a distance of 3.415(2) or 3.4087(5) Å (Figure 3). The tilting of capping Sb atoms is seen in the $LaSb_2$-type structure as well (Figure 6a).[18] The Sn atoms at 3.499(2) and 3.761(3) Å in $LaSn_{0.75}Sb_2$ are probably too distant and too tilted for there to be any bonding interactions. The shorter La−Sn distances of ∼3.4 Å described above are comparable to that found in $LaSn_3$ (3.372 Å).[31] Moreover, the $LaSn_{0.75}Sb_2$ structure is reminiscent of that of the mercury intercalation compound $Hg_{1.24}TiS_2$,[32] which also contains chains of Hg atoms that are best described as nearly neutral rather than cationic. The oxidation state assignment formulated above, which assumes cationic Sn, may thus have to be modified although we are unsure precisely how.

For the moment, we have attempted some simple chemical substitutions to determine whether the $LaSn_{0.75}Sb_2$ phase can be stabilized in other systems. Preparation of several rare-earth analogues has been successful for *RE* = La, Ce, Pr, Nd, and Sm. All of these analogues can support nonstoichiometry of the Sn atoms. Table 6 lists the cell parameters of the compounds prepared from the nominal stoichiometry *RE* + Sn + 2Sb, and should thus correspond to the maximum Sn content in these

(25) Alemany, P.; Alvarez, S.; Hoffmann, R. *Inorg. Chem.* **1990**, *29*, 3070.
(26) Eisenmann, B.; Klein, J. *Z. Naturforsch., B* **1988**, *43*, 69.
(27) Eisenmann, B.; Klein, J. *Z. Naturforsch., B* **1988**, *43*, 1156.
(28) Eisenmann, B.; Klein, J. *Z. Anorg. Allg. Chem.* **1991**, *598/599*, 93.
(29) O'Keeffe, M.; Brese, N. *Acta Crystallogr., Sect. B* **1992**, *48*, 152.
(30) Wells, A. F. *Structural Inorganic Chemistry*, 5th ed.; Clarendon Press: Oxford, U.K., 1984.
(31) Borzone, G.; Borsese, A.; Ferro, R. *Z. Anorg. Allg. Chem.* **1983**, *501*, 199.
(32) Ganal, P.; Moreau, P.; Ouvrard, G.; Sidorov, M.; McKelvy, M.; Glaunsinger, W. *Chem. Mater.* **1995**, *7*, 1132.

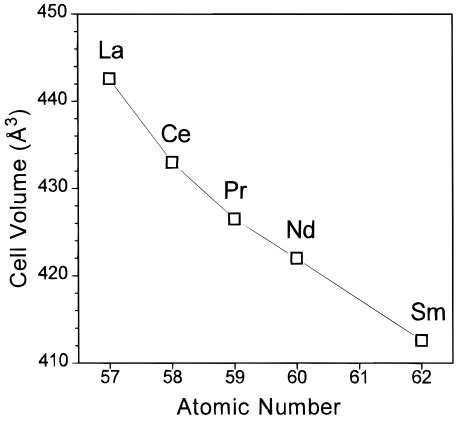

Figure 7. Plot of the unit cell volumes of $LaSn_{0.75}Sb_2$-type compounds obtained from reactions RE + Sn + 2Sb for various rare-earth elements.

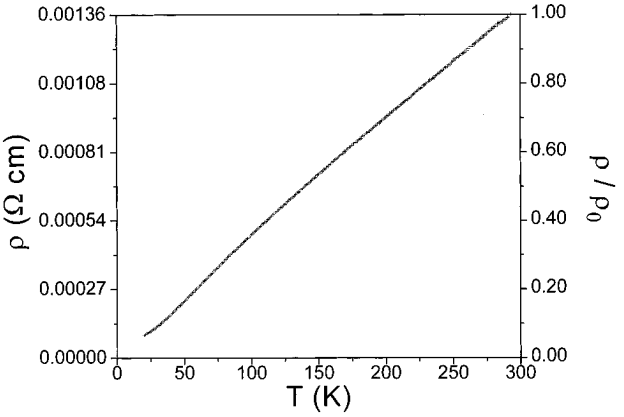

Figure 8. Plot of the electrical resistivity of $LaSn_{0.75}Sb_2$ measured along the needle axis *a*. The left scale refers to the absolute resistivity, and the right scale refers to the resistivity relative to the room-temperature value.

phases. Figure 7 plots the unit cell volume as a function of the rare-earth element. The monotonic decrease of the cell volume is consistent with the expected lanthanide contraction, and the lack of deviation for any of these points implies that the oxidation state of the rare earth is RE^{3+} in all cases. The $LaSn_{0.75}Sb_2$ phase does not form with RE = Gd, suggesting that there may be a link between this result and the curious absence of an ambient pressure $RESb_2$ phase with the late trivalent rare-earth elements RE = Gd−Tm.[18,19] The $LaSb_2$-type phase does form with Gd and Tb, but only at high pressures.[19] It may be worthwhile, therefore, to attempt to prepare the $LaSn_{0.75}Sb_2$ phase with the late rare-earth elements by applying high pressure, as this may be sufficient to overcome unfavorable electrostatic repulsive forces that are enhanced as the structure is contracted by replacement with a smaller rare-earth atom. Substitution with a divalent rare-earth element such as Eu or Yb, if it succeeds, should result in a distorted variant of the $LaSn_{0.75}Sb_2$ structure.

Proceeding to the substitution of the second component, Sn, by its congener Ge, we have discovered a new ternary La/Ge/Sb compound that is *different* from $LaSn_{0.75}Sb_2$.[33] In contrast, preliminary experiments in doping In for Sn have resulted in quaternary compounds $La(In_xSn_y)Sb_2$ that appear to possess the *same* structure as that of $LaSn_{0.75}Sb_2$.[33] This has significant implications for exerting precise electronic control on the structure and properties of this system. Finally, substitution of Sb with As has resulted in a ternary La/Sn/As compound which we have yet to characterize.

Electrical Resistivity. The compound $LaSn_{0.75}Sb_2$ is poorly metallic or semimetallic with a room-temperature resistivity, measured along the needle axis *a*, of $\rho_{293} \approx 1 \times 10^{-3}$ Ω cm. Figure 8 shows a representative plot of the electrical resistivity as a function of temperature. Although the absolute values of the resistivity are imprecise owing to the difficulty in measuring the cross-sectional area of these crystals, the temperature dependence of the relative resistivity, expressed using the room-temperature value as the reference, is highly reproducible among different specimens of $LaSn_{0.75}Sb_2$. The temperature coefficient for the linear portion extending through most of the curve is $\sim 4 \times 10^{-6}$ Ω cm K^{-1}. At low temperatures, $\rho_{20} \approx 1 \times 10^{-4}$ Ω cm, which may be taken to approach the residual resistivity arising from impurity scattering.[34] The resistivity ratio is thus $\rho_{293}/\rho_{20} \approx 10$.

It would be informative to determine the conductivity along the chains of Sn atoms, aligned along the *c* axis; unfortunately, these needle-shaped crystals tend to grow along the *a* axis instead, so the measurements made here correspond to conduction *perpendicular* to these Sn chains but parallel to the square net of Sb(1) atoms. The layered character of the crystal structure portends high electrical anisotropy, and conductivity parallel to the stacking axis *b* is expected to be much weaker than in the other two directions.

Implications. The $LaSn_{0.75}Sb_2$ structure is a highly versatile structure type that can accommodate variable amounts of Sn in the interlayer sites. Clearly it is tempting to classify $LaSn_{0.75}Sb_2$ as an intercalation compound, although formally the host structure $LaSb_2$ itself does not exist with accessible van der Waals gaps, as in the layered dichalcogenides. In fact, the structure of $LaSb_2$ is strongly bonded in the stacking direction, with the layers held together by Sb−Sb bonds.[18] Perhaps an alternative term that better describes the $LaSn_{0.75}Sb_2$ structure is that of a symbiotic guest−host relationship between a $LaSb_2$ substructure and the Sn guest atoms. A simple experiment to try is to see if the reaction $LaSb_2$ + Sn also results in the ternary phase, for this would show if the formation of $LaSn_{0.75}Sb_2$ is as literal as implied by Figure 6, with initial breaking of Sb−Sb bonds followed by insertion of the Sn atoms.

Given the common usage of Sn as a high-temperature flux to promote crystal growth of solid-state compounds, particularly pnictides,[35] it is surprising that this ternary compound has never been properly characterized before. The compound identified by Wang *et al.* as "$LaSnSb_2$" was suggested,[11] correctly, to have a structure similar to that of $NdTe_3$,[12] which also possesses layers of square-antiprismatic rare-earth atoms and square Te sheets. However, the elongated 26 Å axis of $NdTe_3$ arises from the insertion of an additional Te sheet, whereas the elongated 23 Å axis of $LaSn_{0.75}Sb_2$ arises from the insertion of the Sn chains. We have thus shown that the structure of this phase is much more interesting than was originally postulated.

The unusual feature of the Sn chains should be investigated further. The Sn sites probably represent discrete local energy minima, and the potential energy barriers for a Sn atom to jump from one site to another ought to be low. The structure thus appears to satisfy the criteria for high mobility of the Sn atoms through open channels. Since the Sn content can be varied over a wide range, we would like to find out whether Sn atoms can be reversibly inserted or removed.

In summary, the $RESn_xSb_2$ system provides a rare opportunity to exert formidable electronic and steric control on an unusual low-dimensional structure. Not only does it support a wide

(33) Unpublished results.
(34) Ashcroft, N. W.; Mermin, N. D. *Solid State Physics*; Saunders: Philadelphia, 1976.
(35) von Schnering, H.-G.; Hönle, W. *Chem. Rev.* **1988**, *88*, 243.

range of nonstoichiometry of the Sn atoms, but it is also amenable to a variety of chemical substitutions. With rare-earth atoms that have partially-filled f subshells, low-dimensional magnetic ordering phenomena are expected. Doping experiments in which some of the rare-earth atoms are substituted by alkaline-earth atoms are under way. Further experiments to characterize the Sn atoms and to measure electrical properties as a function of Sn content are also in progress. It would be particularly interesting to calculate the electronic band structure of these compounds to elucidate the driving forces for the filling of the Sn sites, and we are currently planning to do this.

Acknowledgment. This work was supported by the Natural Sciences and Engineering Research Council of Canada and the University of Alberta. We are grateful to Dr. Robert McDonald (Faculty Service Officer, Structure Determination Laboratory) for the data collection and to Mr. Wei-Min Chen and Dr. John Beamish for assistance in the resistivity measurements.

Supporting Information Available: Tables S1 and S2, listing further experimental details and anisotropic displacement parameters (3 pages). Ordering information is given on any current masthead page.

IC9602254